Int. J. Appl. Math. Comput. Sci., 2009, Vol. 19, No. 3, 485–499
DOI: 10.2478/v10006-009-0039-x

amcs

DERIVATION OF PHYSICALLY MOTIVATED CONSTRAINTS FOR EFFICIENT INTERVAL SIMULATIONS APPLIED TO THE ANALYSIS OF UNCERTAIN DYNAMICAL SYSTEMS

MAREILE FREIHOLD, EBERHARD P. HOFER

Institute of Measurement, Control, and Microtechnology
University of Ulm, D-89069 Ulm, Germany
e-mail: m.freihold@web.de, eberhard.hofer@uni-ulm.de

Interval arithmetic techniques such as VALENCIA-IVP allow calculating guaranteed enclosures of all reachable states of continuous-time dynamical systems with bounded uncertainties of both initial conditions and system parameters. Considering the fact that, in naive implementations of interval algorithms, overestimation might lead to unnecessarily conservative results, suitable consistency tests are essential to obtain the tightest possible enclosures. In this contribution, a general framework for the use of constraints based on physically motivated conservation properties is presented. The use of these constraints in verified simulations of dynamical systems provides a computationally efficient procedure which restricts the state enclosures to regions that are physically meaningful. A branch and prune algorithm is modified to a consistency test, which is based on these constraints. Two application scenarios are studied in detail. First, the total energy is employed as a conservation property for the analysis of mechanical systems. It is shown that conservation properties, such as the energy, are applicable to any Hamiltonian system. The second scenario is based on constraints that are derived from decoupling properties, which are considered for a high-dimensional compartment model of granulopoiesis in human blood cell dynamics.

Keywords: VALENCIA-IVP, consistency tests for the reduction of overestimation, identification of dynamical constraints, Hamiltonian systems, branch and prune algorithms.

1. Introduction

VALENCIA-IVP is a verified solver for sets of ordinary differential equations (ODEs) that allows for bounded uncertainties in the initial states and system parameters (Rauh *et al.*, 2007). The uncertainties are considered through the use of interval arithmetic, the advantage hereby being that calculations always result in guaranteed enclosures (Moore, 1964). In naive implementations, the enclosures might be too conservative. All reachable states of a dynamical system which are subject to the above mentioned uncertainties are guaranteed to be included in enclosures calculated by VALENCIA-IVP. In order to obtain an enclosure which is less conservative, overestimation has to be detected and reduced. The difficulty of dealing with overestimation is a problem that is also addressed by other verified ODE solvers, e.g., by preconditioning strategies implemented in VNODE or by the Taylor model arithmetic used in COSY VI (Nedialkov, 2007). In this paper, a tighter enclosure of the exact solution is achieved by defining physically motivated constraints which identify regions in the state space that are meaningless. Any enclosure that spreads into these regions can be reduced since it is caused by overestimation. A basic approach which identifies constraints to reduce overestimation in verified simulations of sets of ODEs was published in (Singer and Barton, 2006).

In order to implement an approach which is applicable to a large class of dynamical systems, a general framework for the identification of constraints has to be defined. For applications in mechanics, this framework is based on the Hamiltonian system formulation (van der Schaft and Maschke, 2003), using the conservation law of energy as its basic principle. These constraints are used to identify which parts of the state enclosures are caused by overestimation. In this paper, a branch and prune algorithm (Clausen, 1999; de Figueiredo *et al.*, 1997) is developed and implemented in VALENCIA-IVP as a consistency test that confines the state enclosure with the aid of the constraints to physically meaningful areas. It aims

at enclosing the exact set of solutions under consideration of all uncertainties of initial conditions and parameters as precisely as possible.

The applicability of the branch and prune algorithm is demonstrated on two dynamic systems with uncertainties. The first one is a double pendulum. In this case, the constraints are based on the law of conversation of energy. As an example of a high-dimensional dynamical system, a biomathematical model of blood cell growth according to Fliedner and Steinbach (Hofer *et al*., 1991b) is analyzed as a second application. The constraints are based on the decoupling of cell compartments, such that the internal exchange of cells does not influence the input and output variables explicitly. The complexity and the high dimensionality of these two models manifest that VALENCIA-IVP and the newly implemented branch and prune algorithm are applicable to a wide class of mechanical and biomathematical problems.

This paper is structured as follows: A general overview of VALENCIA-IVP is given in Section 2. Possible constraints and how they can be applied to Hamiltonian systems are discussed in Sections 3 and 4. The branch and prune algorithm is modified to a consistency test in Section 5. Two applications are studied in detail to highlight the use of the newly implemented consistency test in VALENCIA-IVP in Sections 6 and 7. Finally, the paper is concluded with an outlook on future research.

2. VALENCIA-IVP

VALENCIA-IVP is a verified solver for initial value problems (IVPs) for ODEs (Rauh, 2008; Rauh *et al*., 2007). It has the ability to work with interval variables which result from the propagation of uncertain initial conditions and uncertain parameters. The stipulation for VALENCIA-IVP, as with all other verified ODE solvers such as VNODE, VSPODE, or COSY VI, is that guaranteed bounds for the initial conditions and for all uncertain parameters are known. In VALENCIA-IVP, interval arithmetic techniques are applied to determine the worst-case influence of selected parameters on the state variables. Calculations with intervals can lead to overestimation, and VALENCIA-IVP has several mechanisms implemented which are able to detect and reduce overestimation.

2.1. Systems under consideration. VALENCIA-IVP has been developed for systems of continuous-time ODEs,

$$\dot{x}_s(t) = f_s(x_s(t), p(t), t), \tag{1}$$

with the state vector $x_s(t) \in \mathbb{R}^{n_s}$, the vector $p(t) \in \mathbb{R}^{n_p}$ of system parameters, and the nonlinear state-space representation $f_s : D \mapsto \mathbb{R}^{n_s}$, $D \subset \mathbb{R}^{n_s} \times \mathbb{R}^{n_p} \times \mathbb{R}^1$. In the equation (1), the vector $p(t)$ may be time-varying. In this case, parameter variations are expressed by additional ODEs,

$$\dot{p}(t) = \Delta p(t), \tag{2}$$

with $\Delta p(t) \in \left[\underline{\Delta p}; \overline{\Delta p}\right]$ and $p(t) \in \left[\underline{p}; \overline{p}\right]$. The definition of an extended state vector

$$x(t) := \begin{bmatrix} x_s(t) \\ p(t) \end{bmatrix} \tag{3}$$

leads to the time-varying dynamic system model

$$\dot{x}(t) = f(x(t), t), \tag{4}$$

which is studied in the following. In VALENCIA-IVP, the systems under consideration only have to be continuously differentiable up to the order 1 in contrast to other solvers such as VNODE, which demand differentiability up to the order of the interval Taylor series expansions applied.

2.2. Calculation of guaranteed state enclosures. The guaranteed state enclosure

$$[x_{\text{encl}}(t)] := x_{\text{app}}(t) + [R(t)] \quad \text{for} \quad t \in [t_0; t_f] \tag{5}$$

that is calculated in VALENCIA-IVP is generated via a two-stage approach. First, a suitable approximate solution $x_{\text{app}}(t)$ is computed using arbitrary non-verified ODE solvers, e.g., relying on explicit/implicit Euler methods or Runge-Kutta methods. Then, verified error bounds $[R(t)]$ are determined using an iteration procedure which can be derived using Banach's fixed-point theorem. A detailed explanation of this two-stage approach together with its proof can be found in (Rauh, 2008; Rauh *et al*., 2007). For further information, see also (Rauh *et al*., 2009).

3. Constraints

Physical constraints derived from dynamic system models provide additional information about the reachability of certain regions in the state space. This information is used to restrict the solution space to feasible regions of the state space, in other words, to detect overestimation. The goal of consistency tests is to reduce the overestimation that is encompassed by the guaranteed state enclosure $[x_{\text{encl}}(t)]$. In the following subsections, examples of physically motivated constraints relevant to the application scenarios considered in this paper are summarized.

3.1. Energy as a constraint. Conservation laws account for physically measurable properties in a closed system such as the energy, the momentum, or the electric charge through balance equations. In mechanics, the total energy

$$E = E_{\text{kin}} + E_{\text{pot}} \tag{6}$$

of a closed system is constant if the system is subject neither to energy dissipation nor to external gain of energy. Overestimation can be detected due to the violation

of constraints and eliminated in suitable consistency tests. It is known that all admissible solutions, and thus also the exact solutions, are restricted to physically meaningful areas.

3.2. Generalized coordinates. In mechanical system models, generalized coordinates are a suitable coordinate system to describe the equations of motion. The generalized coordinates in which the constraints are defined are denoted by q_i with $i = 1, \ldots, s$, where s is equal to the degrees of freedom in the system model. The generalized coordinates have to be independent of each other, representing the location of each body in a mechanical system model. They are widely used in modeling multibody dynamics using the Denavit-Hartenberg conventions (Pfeiffer and Reithmeier, 1987).

3.3. General constraints. Hamiltonian system formulations can also be derived for electrical as well as electromechanical applications. Using these formulations, the class of systems can be extended and conservation properties can be derived and applied to detect and reduce overestimation in verified simulations. Furthermore, Port-Hamiltonian system representations (van der Schaft and Maschke, 2003), which are a generalization of energy-based system models, can be considered. Since Port-Hamiltonian formulations are the basis for several modern approaches for stability-based control of nonlinear systems, the corresponding mathematical models are often readily available to be applied to analyze the influence of parameter uncertainties using interval arithmetic techniques for the systems' open-loop as well as closed-loop dynamics.

4. Hamiltonian systems

The Hamiltonian mechanism is a re-formulation of classical mechanics which describes the motion of objects with the aid of Newton's laws. The Hamiltonian

$$H = E_{\text{kin}} + E_{\text{pot}} \tag{7}$$

is equal to the total energy of a closed system, with the kinetic energy $E_{\text{kin}} =: K$ and the potential energy $E_{\text{pot}} =: P$. The advantage of using the Hamiltonian formulation is that it allows us to describe complex dynamic systems systematically. The Hamiltonian is defined in terms of the generalized coordinates q.

4.1. Aim of the Hamiltonian system. This section describes the derivation of the expression for the Hamiltonian for a given mechanical system. The Hamiltonian system representation is applied to exploit conservation constraints and balance equations. The goal is to generate a three-stage sequence

$$\underbrace{q\,,\dot{q}\,,M}_{\text{Step 1}} \longrightarrow \underbrace{K\,,P}_{\text{Step 2}} \longrightarrow \underbrace{H\,,\dot{H}}_{\text{Step 3}} \tag{8}$$

in order to derive constraints automatically such that they can be applied in VALENCIA-IVP to detect and reduce overestimation. Step 1 is the description of a dynamical system using generalized coordinates out of which an expression for the energy (Step 2) and its time derivative (Step 3) can be formed.

The Hamiltonian H and the integration of its time derivative $\dot{H}$ that are obtained in Step 3 are physically identical. The different mathematical representations of their calculation introduce different types of overestimation that are caused by the use of interval arithmetic. This information is used for a consistency test based on a branch and prune algorithm. In the following, the constraints are denoted by $H(x)$. The two different ways how the constraints are calculated in VALENCIA-IVP are outlined. The first one is through the solution of additional ordinary differential equations for $H(x(t))$ with

$$H(x(t)) = H(x(0)) + \int_0^t \dot{H}(x(\tau))\,\mathrm{d}\tau\ , \tag{9}$$

by verified integration of the time derivative $\dot{H}(x(t))$ of the Hamiltonian. The term $H(x(0))$ is determined for the given enclosure $[x(0)]$ of the initial states $x(0)$. This constraint is referred to as the VALENCIA-IVP constraint H_V. The second way is the calculation of the Hamiltonian $H(x(t))$ directly as a function of the state vector as its basic principle. This constraint is also calculated in VALENCIA-IVP for the verified enclosures $[x_{\text{encl}}(t)]$ and is called the Hamiltonian constraint H_H.

4.1.1. Calculation of Step 1. Through the use of physically motivated techniques, the generation of an energy equation should be applicable to any mechanical system, as long as the state equation (4) is given in terms of a dynamic system model consisting of a symmetric and positive definite mass matrix $M(q) \in \mathbb{R}^{s\times s}$, generalized coordinates q, $\dot{q}$, $\ddot{q}$, and a generalized force vector $\tau = [\tau_1, \ldots, \tau_s]^T$. It is necessary that the mass matrix be both positive definite and symmetric, such that $M(q) = M^T(q)$ and $M^{-1}(q) = (M^{-1}(q))^T$ hold. However, it may be an arbitrary function of q.

4.1.2. Calculation of Step 2. The kinetic energy K and the potential energy P in Step 2 are calculated by the results of Step 1 with the use of the Hamiltonian equations of motion. These equations consist of

$$\dot{q} = \frac{\partial H(q,p)}{\partial p} = M^{-1}(q)\cdot p, \tag{10}$$

and

$$\dot{p} = -\frac{\partial H(q,p)}{\partial q} + \tau, \tag{11}$$

which form a set of coupled ODEs for the generalized coordinates q and the generalized momenta $p = [p_1, \ldots, p_s]^T$. The expression for the kinetic energy

$$K(q,\dot{q}) = \frac{1}{2} \cdot \dot{q}^T \cdot M(q) \cdot \dot{q} \tag{12}$$

results directly from the information obtained in Step 1. The derivation for the equation of the potential energy is far more complex, if it is not given analytically. For the derivation of the potential energy, the kinetic energy (12) needs to be defined in terms of the generalized momenta p and the generalized coordinates q resulting in

$$K(q,p) = \frac{1}{2} \cdot p^T \cdot M^{-1}(q) \cdot p, \tag{13}$$

with

$$p = M(q) \cdot \dot{q}. \tag{14}$$

With these definitions, the Hamiltonian for the derivation of the potential energy is given by

$$H(q,p) = \frac{1}{2} \cdot p^T \cdot M^{-1}(q) \cdot p + P(q), \tag{15}$$

explicitly depending on q and p. The time derivative of the generalized momenta determined from (14) is set equal to the expression (11). The expression (15) for the Hamiltonian is substituted for H in the equation (11) leading to

$$\dot{p} = -\frac{\partial}{\partial q}\Big(\frac{1}{2} \cdot p^T \cdot M^{-1}(q) \cdot p + P(q)\Big) + \tau \stackrel{!}{=} \frac{\mathrm{d}}{\mathrm{d}t}\Big(M(q) \cdot \dot{q}\Big) \tag{16}$$

and solved for the partial derivative $\frac{\partial P(q)}{\partial q}$ of the potential energy $P(q)$ according to

$$\frac{\partial P(q)}{\partial q} = -\frac{\partial}{\partial q}\Big(\frac{1}{2} \cdot p^T \cdot M^{-1}(q) \cdot p\Big) + \tau - \frac{\mathrm{d}}{\mathrm{d}t}\Big(M(q) \cdot \dot{q}\Big). \tag{17}$$

The integral of (17) provides the missing expression for the potential energy according to

$$\begin{aligned} P_i(q) &= \int \Bigg(-\frac{\partial}{\partial q_i}\Big(\frac{1}{2} \cdot p^T \cdot M^{-1}(q) \cdot p\Big) \\ &\quad + \tau - \frac{\mathrm{d}}{\mathrm{d}t}\Big(e_i^T \cdot M(q) \cdot \dot{q}\Big)\Bigg) \cdot \mathrm{d}q_i \\ &= \int \Bigg(\frac{1}{2} \cdot \dot{q}^T \cdot \frac{\partial M}{\partial q_i} \cdot \dot{q} \\ &\quad + \tau - \frac{\mathrm{d}}{\mathrm{d}t}\Big(e_i^T \cdot M(q) \cdot \dot{q}\Big)\Bigg) \cdot \mathrm{d}q_i \end{aligned} \tag{18}$$

with $i = 1, \ldots, s$. In (18), each expression $P_i(q)$ represents the potential energy except for terms depending only on $q_1, \ldots, q_{i-1}, q_{i+1}, \ldots, q_s$. Each P_i needs to be calculated in order to be able to determine the corresponding integration constants except for arbitrary additive terms which do not depend on any q_i. The combination of all P_i, $i = 1, \ldots, s$, results in a complete representation of the potential energy $P(q)$. In general, Step 2 can be evaluated with (13) and (18).

4.1.3. Calculation of Step 3. From Step 2, the constraints H and $\dot{H}$ that are used in VALENCIA-IVP can be computed. The interval evaluation of physically identical constraints is used to detect overestimation that is caused by the different mathematical evaluations. The implemented consistency test in Section 5 can use the constraints to detect overestimation.

4.2. Internal and external influence on the systems. For a closed system, meaning that there is no internal or external loss or gain of energy ($\tau = 0$), the time derivative of the energy balance

$$\begin{aligned} \frac{\mathrm{d}}{\mathrm{d}t}H(q,p) &= \frac{\partial^T H(q,p)}{\partial q} \cdot \dot{q} + \frac{\partial^T H(q,p)}{\partial p} \cdot \dot{p} \\ &= \frac{\partial^T H(q,p)}{\partial p} \cdot \tau = \dot{q}^T \cdot \tau \end{aligned} \tag{19}$$

results in

$$\frac{\mathrm{d}}{\mathrm{d}t}H = 0. \tag{20}$$

This can be used as additional information for formulating the constraints. In the general case the time derivative of the energy of an open system ($\tau \neq 0$) is usually not equal to zero.

4.3. Further consistency tests. The consistency test that is based on a branch and prune algorithm, see Section 5, can reduce the overestimation that is identified by the constraints. However, it can only detect overestimation that occurs in the state variables that are considered in the constraints. That is the reason why the backward integration consistency test that is implemented in VALENCIA-IVP still needs to be used (Rauh, 2008; Rauh *et al.*, 2007). The backward integration of subintervals is computationally more expensive than the consistency test described in the following. It is therefore beneficial to reduce overestimation as much as possible beforehand with the branch and prune consistency test.

5. Branch and prune algorithm

A modified branch and prune algorithm is implemented as a consistency test in VALENCIA-IVP in order to detect and reduce overestimation.

5.1. Background information. Branch and bound algorithms are general numerical techniques for solving box-constrained global optimization problems (Kearfott, 1992). Given is a box Ω with n dimensions, corresponding to the dimension of the problem (Boyd *et al.*, 2003). The branch and bound method consists of two parts. The branching is the subdivision of Ω into smaller subregions and the bounding is the computation of the lower and upper bounds of the global minimum of a cost function. The branch and bound algorithm is often compared to a dynamically growing tree (Boyd *et al.*, 2003) in which the original box is the root and each subregion of Ω belongs to a branch further into the tree. The goal is to narrow down the region in which the global optimum lies while discarding large subregions which cannot contain the global optimum. This procedure is called pruning as those branches are not further explored. The branches that are still up for further investigation are written in a list $\mathcal{L}$, so that at any time the list $\mathcal{L}$ contains a verified solution of the problem (de Figueiredo *et al.*, 1997).

5.2. Application. The branch and prune algorithm that is implemented in VALENCIA-IVP is not used to find a global minimum. It rather finds intervals that conform to the constraints motivated in Section 4. The constraints can be viewed as an optimization function. If an interval conforms to the VALENCIA-IVP constraint H_V, then it is an "optimal" interval. If it does not, then it either has to be split up into smaller intervals according to a subdivision strategy or it can be discarded.

Based on dichotomic branching, each branch generates two new branches. The evaluation of the Hamiltonian constraint H_H tests if each branch is either within the bounds, partially outside, or completely outside the allowed range which is given by the guaranteed enclosure of the VALENCIA-IVP constraint H_V. These intervals are distinguished as `true`, `undecided`, or `false` branches. A `false` branch corresponds to a pruned branch in which the optimum does not lie, see the reduction area in Section 5.4. In Fig. 1, an example tree is drawn for three stages. For each branch in each stage, the Hamiltonian constraint H_H has to be calculated and compared to the VALENCIA-IVP constraint H_V. Figures 2 and 3 illustrate the relationship between the intervals `true`, `undecided`, and `false` and the constraints. A `false` interval is a branch that is pruned because it lies completely outside the VALENCIA-IVP constraint H_V. It is not further investigated.

The rest of the branches are written in a list $\mathcal{L}$, which contains all branches that represent `undecided` or `true` intervals. The `undecided` intervals are further branched until they either yield decisive results or a stopping criterion has been reached.

In the case of multiple constraints, i.e., $m > 1$, a branch is discarded if at least one constraint leads to a `false` interval. It is classified as an `undecided` interval if the constraints represent a mixture of `true` intervals and at least one `undecided` interval but no `false` ones.

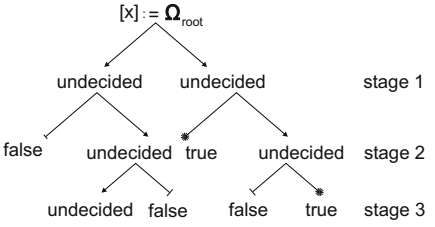

Fig. 1. Example tree in which each branch is tested for consistency.

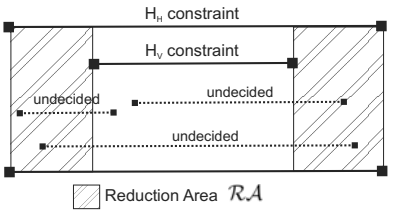

Fig. 2. `Undecided` intervals can have a smaller infimum or a larger supremum (or both) than the VALENCIA-IVP constraint H_V.

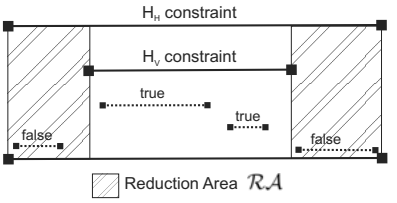

Fig. 3. `True` intervals lie completely within the VALENCIA-IVP constraint H_V. `False` intervals do not intersect with the VALENCIA-IVP constraint H_V.

5.3. Subdivision strategies. In VALENCIA-IVP, six different subdivision strategies are implemented. The user can choose an appropriate strategy according to the system under consideration. The overall goal is to split branches efficiently into two new subregions. The subdivision occurs at the midpoint for a single component x_{j^*}, $j^* \in \{1, \ldots, n\}$, of the state vector x. All other components are identical to the original box. The component x_{j^*} is the one that maximizes the criterion of the subdivision method and it is split into two new regions,

$$[x_{i,low}] := \begin{cases} [x_i] & \text{for} \quad i \neq j^*, \\ [\inf([x_{j^*}]); \text{mid}([x_{j^*}])] & \text{for} \quad i = j^*, \end{cases} \tag{21}$$

and

$$[x_{i,upp}] := \begin{cases} [x_i] & \text{for} \quad i \neq j^*, \\ [\text{mid}([x_{j^*}]); \sup([x_{j^*}])] & \text{for} \quad i = j^*. \end{cases} \tag{22}$$

The preceding section only considered the scalar case, $m = 1$. For multiple constraints, the terms H_l, $l = 1, \ldots, m$, are distinguished, where m equals the number of constraints. The following subdivision strategies aim at improving the splitting direction by taking into account the variation of the constraints in all components of the state vector.

5.3.1. Strategy 1: Subdivision along the longest edge. The component

$$j^* = \underset{i=1,\ldots,n}{\arg\max} \big(\text{diam}\big\{[x_i]\big\}\big) \tag{23}$$

of the state vector with the largest width is chosen for splitting. The subdivision strategies 2–6 aim at improving the splitting direction by taking into account the variation of the constraints in all components of the state vector.

5.3.2. Strategy 2: Subdivision along the largest change of the derivative w.r.t. the state variables. The Jacobian matrix

$$[J] := \left[\begin{array}{ccc} \frac{\partial H_1}{\partial x_1} & \cdots & \frac{\partial H_1}{\partial x_n} \\ \vdots & \ddots & \vdots \\ \frac{\partial H_m}{\partial x_1} & \cdots & \frac{\partial H_m}{\partial x_n} \end{array}\right]\Bigg|_{x=[x]} \tag{24}$$

of the constraints H_l, $l = 1, \ldots, m$, is determined for the state vector, using automatic differentiation provided by FADBAD++ (Bendsten and Staunting, 2007). Each row of the Jacobian matrix corresponds to one of the constraints $H_{H,l}$, and the columns amount to the number of components of the state vector. The decision is based on the diameter

$$\text{diam}\left\{\left[\frac{\partial H_l}{\partial x_i}\right]\right\} \cdot \text{diam}\left\{[x_i]\right\}, \tag{25}$$

for $l = 1, \ldots, m$ and $i = 1, \ldots, n$ of each entry of the Jacobian matrix. Scaling with the diameter of the state variable x_i prevents bias towards a state variable with negligible width. This helps to avoid a situation when the same state variable would be chosen numerously. The argument that maximizes the corresponding component

$$j^* = \underset{i=1,\ldots,n}{\arg\max} \left(\max_{l=1,\ldots,m} \left\{ \text{diam}\Big\{[J_{l,i}]\Big\} \cdot \text{diam}\big\{[x_i]\big\} \right\} \right) \tag{26}$$

of the state vector gets chosen to be split. This is the component of the state vector with the greatest sensitivity based on the entire interval.

5.3.3. Strategy 3: Subdivision in the direction determined by the largest change in the center of the state enclosure. In this subdivision strategy, the Jacobian matrix is evaluated for the midpoint of the state enclosure

$$[M] := \left[\begin{array}{ccc} \frac{\partial H_1}{\partial x_1} & \cdots & \frac{\partial H_1}{\partial x_n} \\ \vdots & \ddots & \vdots \\ \frac{\partial H_m}{\partial x_1} & \cdots & \frac{\partial H_m}{\partial x_n} \end{array}\right]\Bigg|_{x=\text{mid}([x])} \tag{27}$$

yielding a point matrix instead of an interval matrix like before. Instead of forming the diameter of each entry, the absolute magnitude for a scalar interval $[x]$ is calculated which is defined by

$$\text{abs}\left\{[x]\right\} := \max\left\{|\underline{x}|\,; |\overline{x}|\right\} \tag{28}$$

in the PROFIL/BIAS V 2.0.4. (Keil, 2007). This is the definition that is used for the absolute magnitude in this paper. This definition is applied component-wise to vectors or matrices. Note that the standard definition of the absolute magnitude for interval variables is as follows:

$$\text{abs}\left\{[x]\right\} := \begin{cases} [0; \max\left\{|\underline{x}|\,, |\overline{x}|\right\}] & \text{for} \quad 0 \in [x]\,, \\ [\min\left\{|\underline{x}|\,, |\overline{x}|\right\}; \max\left\{|\underline{x}|\,, |\overline{x}|\right\}] & \text{otherwise.} \end{cases} \tag{29}$$

Each entry of the matrix is scaled with the diameter of the corresponding state variable to avoid bias. The largest entry

$$j^* = \underset{i=1,\ldots,n}{\arg\max} \left(\max_{l=1,\ldots,m} \left\{ \text{abs}\Big\{[M_{l,i}]\Big\} \cdot \text{diam}\big\{[x_i]\big\} \right\} \right) \tag{30}$$

now represents the direction of the largest change out of the center of the interval box.

5.3.4. Strategy 4: Subdivision based on the magnitude of the change of the state variables. The Jacobian matrix is calculated again for the complete state enclosures. The maximizing component

$$j^* = \underset{i=1,\ldots,n}{\arg\max} \left(\max_{l=1,\ldots,m} \left\{ \text{abs}\Big\{[J_{l,i}]\Big\} \cdot \text{diam}\big\{[x_i]\big\} \right\} \right) \tag{31}$$

is determined for each state variable in all Hamiltonian constraints. It is scaled with the corresponding diameter of the state enclosure with the definition of the absolute magnitude in the equation (28). The state variable chosen for splitting is the one with the largest magnitude of change.

5.3.5. Strategy 5: Subdivision based on each individual edge, along the edge with the largest change. This

$$\mathcal{X} := \begin{cases} [\underline{x}_1, \underline{x}_2, \ldots, \underline{x}_{i-1}, [x_i], \underline{x}_{i+1}, \ldots, \underline{x}_n] & \text{entry} \quad \alpha = 1 \\ [\overline{x}_1, \underline{x}_2, \ldots, \underline{x}_{i-1}, [x_i], \underline{x}_{i+1}, \ldots, \underline{x}_n] & \text{entry} \quad \alpha = 2 \quad \ldots \\ [\overline{x}_1, \overline{x}_2, \ldots, \overline{x}_{i-1}, [x_i], \overline{x}_{i+1}, \ldots, \overline{x}_n] & \text{entry} \quad \alpha = n \cdot 2^{n-1} \end{cases} \tag{32}$$

$$j^* = \arg\max_{i=1,\ldots,n} \left(\max_{l=1,\ldots,m} \left\{ \max_{\alpha=1,\ldots,n\cdot 2^{n-1}} \left\{ \operatorname{diam}\left\{ \left[J_{l,i}\Big|_{x=\mathcal{X}_\alpha} \right] \right\} \cdot \operatorname{diam}\left\{ \left[x_i\Big|_{x=\mathcal{X}_\alpha} \right] \right\} \right\} \right) \tag{33}$$

$$j^* = \arg\max_{i=1,\ldots,n} \left(\max_{l=1,\ldots,m} \left\{ \max_{\alpha=1,\ldots,n\cdot 2^{n-1}} \left\{ \operatorname{diam}\left\{ \left[J_{l,i}\Big|_{x=\mathcal{X}_\alpha} \right] \right\} \cdot \operatorname{mid}\left\{ \left[x_i\Big|_{x=\mathcal{X}_\alpha} \right] \right\} \right\} \right) \tag{34}$$

subdivision method is the most elaborate one. The Jacobian matrix is now evaluated for each edge of the state enclosure $[x]$, corresponding to an n-dimensional hypercube. Thus an n dimensional problem has $n \cdot 2^{n-1}$ edges, meaning that this number of computations has to be carried out in order to determine j^*. The index α denotes a single edge with $\alpha \in \{1, \ldots, n \cdot 2^{n-1}\}$. This subdivision method should be carefully chosen and is not suited for high-dimensional problems. An edge of the hypercube is defined through one of the state variables being an interval variable and all other state variables being point intervals. For all possible combinations in (32) with $i = 1, \ldots, n$ and $\alpha = 1, \ldots, n \cdot 2^{n-1}$, the Jacobian matrix is evaluated. It is then scaled with the diameter of the corresponding edge. The index determined in (33) denotes the state variable with the largest change on its edge.

5.3.6. Strategy 6: Subdivision based on each individual edge, scaled with the midpoint of the state enclosures. This method uses the same algorithm as Strategy 5. The only difference is that instead of scaling the Jacobian matrix with the diameter of the corresponding edge, it is scaled with the midpoint of the edge. The index determined in (34) denotes the state variable with the largest change on its edge.

5.4. Reduction area. The subdivision strategies have been introduced. The goal is to find a time instant $t^* \in [t_0; t_f]$ at which the branch and prune algorithm is applied in order for the optimal amount of overestimation to be detected and reduced. The intersection of the VALENCIA-IVP constraint H_V and the Hamiltonian constraint H_H is the tightest possible enclosure of the exact solution, since they are physically the same. If at least one interval bound of the VALENCIA-IVP constraint H_V is tighter than the Hamiltonian H_H constraint, the area that is within the Hamiltonian constraint H_H but outside the VALENCIA-IVP constraint H_V can be eliminated, since the constraints are always computed in a guaranteed way. This area is called the reduction area

$$\begin{aligned} \mathcal{RA}(t) := {} & \operatorname{diam}\{[H_H(t)]\} \\ & - \operatorname{diam}\{[H_H(t)] \cap [H_V(t)]\} \overset{!}{\geq} 0. \end{aligned} \tag{35}$$

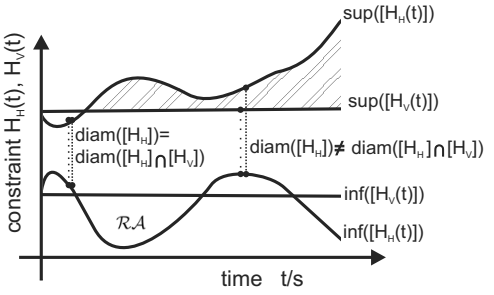

Fig. 4. Arbitrary example to illustrate the reduction area $\mathcal{RA}$.

Figure 4 shows the possible reduction area $\mathcal{RA}$ for an arbitrary example. The behavior of the constraints does not need to be symmetric, meaning that $\inf([H])$ does not need to be symmetric to $\sup([H])$. The only important property is the relation between the Hamiltonian constraint and the VALENCIA-IVP constraint such that a reduction area $\mathcal{RA}$ exists. The relation

$$[H_H] \cap [H_V] \neq \emptyset \tag{36}$$

always holds since the constraints are both guaranteed enclosures of the exact solution. The point of time t^* is chosen such that the reduction area $\mathcal{RA}$ in (35) is maximized according to

$$\mathcal{RA}^* = \max_{t \in [t_0; t_f]} \{\mathcal{RA}(t)\} \ . \tag{37}$$

To simplify the optimization problem, the condition (37) is replaced with a search for the first local maximum in $[t_0; t_f]$. The optimal point of time t^* can be subject to further restrictions that are specific for the system under consideration.

6. Double pendulum

The use of physically motivated techniques to detect and reduce overestimation is illustrated for a double pendulum as an example of mechanical systems. The constraints for this model are defined over its total energy. The double pendulum represents a system assuming ideal conditions. As illustrated in Fig. 5, the double pendulum is composed of two point masses $m_1 = m_2 = 1.0\,\mathrm{kg}$ and two massless

$$\dot{x}(t) = \begin{bmatrix} 1 & 0 & 0 & 0 \\ 0 & 1 & 0 & 0 \\ 0 & 0 & (m_1+m_2)\cdot l_1 & m_2 \cdot l_2 \cdot \cos(x_1(t)-x_2(t)) \\ 0 & 0 & m_2 \cdot l_1 \cdot \cos(x_1(t)-x_2(t)) & m_2 \cdot l_2 \end{bmatrix}^{-1} \cdot \begin{bmatrix} x_3(t) \\ x_4(t) \\ -g\cdot(m_1+m_2)\cdot\sin(x_1(t)) - m_2\cdot l_2 \cdot \sin(x_1(t)-x_2(t))\cdot x_4^2(t) \\ -g\cdot m_2 \cdot \sin(x_2(t)) + m_2 \cdot l_1 \cdot \sin(x_1(t)-x_2(t))\cdot x_3^2(t) \end{bmatrix}. \tag{38}$$

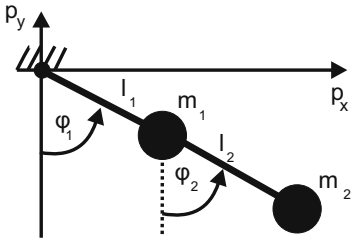

Fig. 5. Double pendulum with masses m_1, m_2, lengths l_1, l_2, and angles φ_1,φ_2.

arms with the lengths of $l_1 = l_2 = 1.0\,\mathrm{m}$. The angles are denoted by φ_1, φ_2 and the gravitational constant by $g = 9.81\,\mathrm{m/s^2}$. A double pendulum has $s = 2$ degrees of freedom, and the generalized coordinates are chosen to be the two angles $q_1(t) := \varphi_1(t)$ and $q_2(t) := \varphi_2(t)$. The state-space model is given in (38), which results from the state vector

$$x(t) = \begin{bmatrix} x_1(t) \\ x_2(t) \\ \dot{x}_1(t) \\ \dot{x}_2(t) \end{bmatrix} := \begin{bmatrix} q_1(t) \\ q_2(t) \\ \dot{q}_1(t) \\ \dot{q}_2(t) \end{bmatrix}, \tag{39}$$

with the angular velocities $x_3(t) = \dot{x}_1(t)$ and $x_4(t) = \dot{x}_2(t)$.

The potential energy of the double pendulum is calculated with the reference potential at the p_x-axis. In general, the reference axis can be chosen arbitrarily since it only affects the energy through a constant additive term. The total energy

$$H_H = K(q,\dot{q}) + P(q) \tag{40}$$

is expressed as the sum of the kinetic energy

$$\begin{aligned} K(q,\dot{q}) = {} & \frac{1}{2}m_1 \cdot \Big((l_1\cos(q_1)\dot{q}_1)^2 + (l_1\sin(q_1)\dot{q}_1)^2\Big) \\ & + \frac{1}{2}m_2 \cdot \Big((l_1\cos(q_1)\dot{q}_1 + l_2\cos(q_2)\dot{q}_2)^2 \\ & + (l_1\sin(q_1)\dot{q}_1 + l_2\sin(q_2)\dot{q}_2)^2\Big) \end{aligned} \tag{41}$$

and the potential energy

$$\begin{aligned} P(q) = {} & m_1 g \cdot \Big(-l_1\cos(q_1)\Big) \\ & + m_2 g \cdot \Big(-l_1\cos(q_1) - l_2\cos(q_2)\Big). \end{aligned} \tag{42}$$

For simplicity, in the notation of the energy of the double pendulum the variables such as the generalized coordinates are not explicitly denoted as time-dependent. The consideration of a closed system, meaning a lack of both energy dissipation and external energy gain, leads to an additional constraint, resulting from the time derivative of the energy

$$\dot{H}_V := \frac{\mathrm{d}E}{\mathrm{d}t} = \left(\frac{\partial E}{\partial q}\right)^T \cdot \dot{q} + \left(\frac{\partial E}{\partial \dot{q}}\right)^T \cdot \ddot{q} = 0, \tag{43}$$

giving

$$H_V = H_V(t) := H_{V,0} = \mathrm{const} \quad \text{for} \quad t \geq 0. \tag{44}$$

With this knowledge, certain areas in the state-space can be defined as physically meaningless in interval simulations of dynamical systems. In calculations with VALENCIA-IVP, overestimation that spreads into these regions can be detected and reduced. Even if it is not possible to symbolically simplify the time derivative of the energy in (43), the result can still be used as a constraint. In that case, the value zero is contained in the interval enclosure of the time derivative of the energy such that $0 \in \left[\dot{H}_V\right]$ holds.

6.1. Simulation results. The implemented branch and prune algorithm has several settings that are analyzed and adjusted to the double pendulum. A pseudo-volume

$$V_{\text{total}} = \prod_{i=1}^{n} \mathrm{diam}\,\{[x_i]\} \tag{45}$$

is introduced in order to compare these simulation results. With this pseudo-volume, the percentage $P_{\texttt{true, undecided}}$ of the volume of the intervals that are `true` or `undecided` can be given by

$$P_{\texttt{true, undecided}} = \frac{V_{\texttt{true}} + V_{\texttt{undecided}}}{V_{\text{total}}} \cdot 100\%. \tag{46}$$

A small percentage $P_{\texttt{true, undecided}}$ of the volume that is kept for further calculations at $t > t^*$ is the desired result. If the percentage $P_{\texttt{true, undecided}}$ is small, then a large amount of overestimation is detected and reduced from further calculations.

For further calculations it is beneficial if the number of the remaining intervals is reduced. This is achieved by merging subintervals. If no means for the limitation of the number of subintervals is used, the number of intervals inevitably grows to the point that a simulation of a dynamical system cannot be calculated anymore (Rauh, 2008).

The simulation results are compared at $t = t^* = 0.45\text{s}$. This is the point of time at which the branch and prune algorithm and the merging routine of VALENCIA-IVP have been applied. Based on the pseudo-volume and the point of time at which the simulations are compared, the results can be discussed. For all the simulations the step size is 0.0002.

6.1.1. Optimal subdivision strategy and the optimal number of subdivisions. Six different subdivision strategies can be chosen from for the system of the double pendulum. Each subdivision strategy is applied 100, 1000, and 10000 times in order to compare the effect of the number of subdivisions. In the case when all subintervals are classified as either `true` or `false`, the subdivision process stops. As long as at least one subinterval is an `undecided` interval, the subdivision process is continued until the maximum number of subdivisions has been reached. In Table 1, the results are listed for an initial enclosure of

$$[x(0)] = \left[\left[0.99 \cdot \frac{3 \cdot \pi}{4}; 1.01 \cdot \frac{3 \cdot \pi}{4}\right], [0.6; 0.6], [0.4; 0.4], [0.7; 0.7]\right].$$

Strategies 1 and 6 are not listed since they did not detect overestimation for the double pendulum. The comparison of the different strategies shows that Strategy 4 is the best subdivision method for the double pendulum. It is able to detect and reduce the largest amount of overestimation for a given number of subdivisions compared with the other strategies. Strategies 5 and 2 are second and third best yielding similar results.

Table 1. Different subdivision strategies are compared on the basis of the percentage $P_{\texttt{true, undecided}}$.

Subdivisions	Strategy 2	Strategy 3	Strategy 4	Strategy 5
100	81.15%	90.63%	73.44%	77.74%
1000	65.59%	70.02%	60.04%	63.00%
10000	55.28%	57.96%	52.34%	53.88%

In general, a larger number of subdivisions results in a larger area that is discarded. VALENCIA-IVP is able to detect more overestimation if more subdivisions take place. An increase in the number of subdivisions affects a decrease in the size of the `true` and `undecided` regions. This can be explained as follows. The chance that a smaller interval conforms or does not conform to the VALENCIA-IVP constraint is higher than that of a larger one. However, the use of a larger number of subdivisions results in a longer computing time and a compromise has to be found. For the double pendulum, a setting of 10000 subdivisions combined with the use of Strategy 4 is a suitable choice.

6.1.2. Variation of the initial enclosure $[x_{2,0}]$. For the following simulations, the effect of different uncertainties for $x_{2,0}$ is analyzed and discussed. The remaining initial state enclosures are identical to Subsection 6.1.1. Subdivision Strategy 4 is used with 10000 subdivisions. These settings are kept constant for the remaining simulations.

The results can be seen in Table 2. The uncertainty of the initial enclosure of $x_{2,0}$ is increased with each simulation in order to be able to analyze the impact of the size of uncertainty for initial values. The different percentages $P_{\texttt{true, undecided}}$ are calculated and recorded for an identical $t = t^*$. In Table 2, the initial enclosures of $x_{2,0}$ with sufficiently small uncertainty yield similar results. A chosen increase in uncertainty shows that VALENCIA-IVP and the newly implemented branch and prune algorithm are capable of detecting and reducing a large region of overestimation. For $x_{2,0} = [0.6; 0.9]$ the largest overestimation region is detected. Figure 6 shows the state enclosure $[x(t^*)]$, the black box, obtained before the branch and prune algorithm. The smaller interval boxes are calculated by the subdivisions and they are the new state enclosure after the application of the consistency test. The corresponding state enclosure of $x_3(t)$ can be seen in Fig. 7. At $t = t^*$, the branch and prune algorithm is applied and this results in a tighter state enclosure for $t > t^*$.

Table 2. Comparison of the effect of differing uncertainty in the initial enclosure $[x_{2,0}]$.

$[x_{2,0}]$	$P_{\texttt{true, undecided}}$
$[0.61000; 0.61001]$	52.31%
$[0.6100; 0.6101]$	52.32%
$[0.610; 0.611]$	52.43%
$[0.61; 0.62]$	53.37%
$[0.6; 0.8]$	50.22%
$[0.6; 0.9]$	42.62%

With the previously determined settings, the simulation results of the double pendulum for the entire VALENCIA-IVP algorithm are analyzed. For an easier comparison of the simulations of the double pendulum with and without the branch and prune algorithm, the vol-

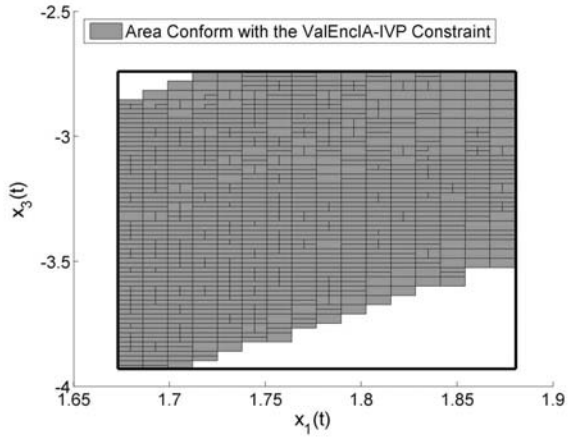

Fig. 6. Reduction area after projection into the (x_1, x_3)-plane with $x_{2,initial} = [0.6; 0.9]$.

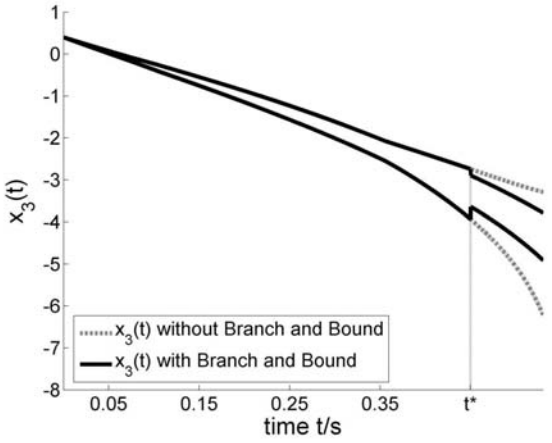

Fig. 7. Enclosure of x_3.

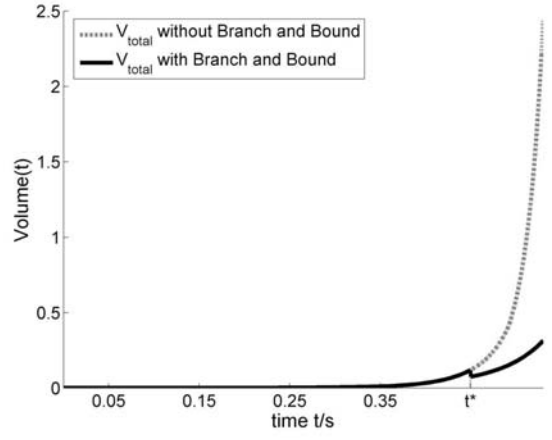

Fig. 8. Pseudo-volume of the state enclosures for simulations with and without the branch and prune algorithm.

umes of the corresponding state enclosures according to the equation (45) are depicted in Fig. 8. The volume of the simulation with the branch and prune algorithm shows a reduction of approximately 90% at $t = 0.55\,\mathrm{s}$ compared with the simulation without the branch and prune algorithm. This detection and reduction of overestimation enables the simulations in VALENCIA-IVP after $t > t^*$ to work with a tighter enclosure of the exact solution set.

6.2. Summary. For the mechanical system of the double pendulum, the Hamiltonian constraints are implemented in order to detect physically meaningless areas. It has been illustrated that VALENCIA-IVP is able to detect and reduce overestimation regardless of the uncertainty of the initial conditions. The double pendulum is a complex system that can show chaotic behavior which is not asymptotically stable. VALENCIA-IVP has been successfully used for detecting and reducing overestimation for this application.

7. Human blood cell dynamics

The next system that is investigated is the biomathematical model of granulopoiesis, a dynamical model for the human blood cell system. The model can be used to assess the damage to the blood renewal system that is caused by several illnesses such as leukemia or when the patient has been exposed to radioactive material, e.g., during accidents in nuclear power plants such as in the Chernobyl accident. The quantification of the damage can help to assist medical doctors in the classification of the damage (Hofer *et al.*, 1991a). A prerequisite for this model is a suitable parameterization.

7.1. Fliedner and Steinbach model. Fliedner and Steinbach came up with a model for granulopoiesis consisting of a set of nonlinear coupled ODEs. Granulopoiesis is the renewal of granulocytes, which make up about 70% of the white blood cells. The renewal process can be viewed as a dynamical system in which the cells undergo several changes in order to develop into granulocytes. All blood cells originate from the *pluripotent stem cells* (S), from which the cell grows until it reaches the circulating blood, represented by the *function compartment* (F). The stages in between are the *compartment bone marrow* (CBM) and the *compartment blood* (CBL), then the *precursor* (P), the *mature* (M), and the *reserve cells* (R) (*The American Heritage Medical Dictionary*, 2007). The schematic set up of granulopoiesis leads to the Fliedner and Steinbach model, which is depicted in Fig. 9, expressing granulopoiesis in terms of cell and information flow. The mathematical description of granulopoiesis is introduced in the following. Each of the compartments CBL, CBM, and P is subdivided into 10 subcompartments, each

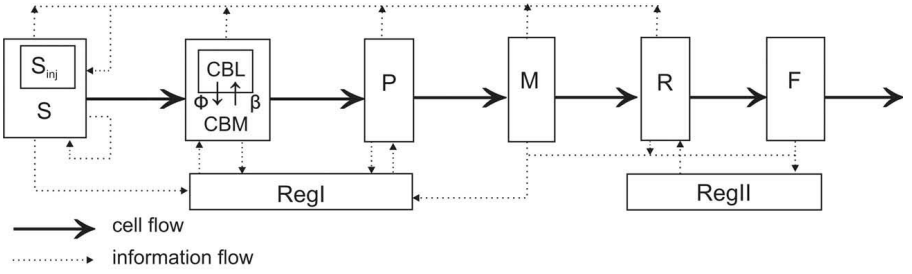

Fig. 9. Model of granulopoiesis according to Fliedner and Steinbach.

without direct medical or biological meaning. The state variables

$$\begin{aligned}
x_1 &= S,\\
x_2 &= CBM_1 \quad ,\ldots, \quad x_{11} = CBM_{10},\\
x_{12} &= CBL_1 \quad ,\ldots, \quad x_{21} = CBL_{10},\\
x_{22} &= P_1 \quad ,\ldots, \quad x_{31} = P_{10},\\
x_{32} &= M,\\
x_{33} &= R,\\
x_{34} &= F,\\
x_{35} &= RegI,\\
x_{36} &= RegII
\end{aligned} \tag{47}$$

represent the seven different compartments of the granulopoiesis modeled according to Fliedner and Steinbach, as well as the two hormonal regulators $RegI$ and $RegII$ (Hofer *et al*., 1991b). After introducing the abbreviations

$$\begin{aligned}
u_a &= -\nu_2 \cdot (x_2 + \cdots + x_{11} + x_{22} + \cdots + x_{33}),\\
u_1 &= \gamma_1 \exp(-\nu_1 x_1) + \gamma_2 \exp(u_a) + \gamma_3,\\
u_2 &= \gamma_4 - \gamma_5 \exp(-\nu_3 x_{35}),\\
u_3 &= 2(1-\rho) u_1 x_1,\\
u_4 &= \beta,\\
u_5 &= \lambda_c x_{11},\\
u_6 &= \gamma_6 - \gamma_y \exp(-\nu_4 x_{35}),\\
u_7 &= \lambda_p x_{31},\\
u_8 &= \gamma_8 - \gamma_9 \exp(-\nu_5 x_{36}),\\
u_9 &= u_8 x_{33},\\
u_b &= g_2 \cdot (x_2 + \cdots + x_{11}),\\
u_c &= g_3 \cdot (x_{22} + \cdots + x_{34}),\\
u_{10} &= \gamma_{10} \exp\Big(-\nu_6 \cdot \big(g_1 x_1 + u_{10b} + u_{10c}\big)\Big),\\
u_{11} &= \gamma_{11} \exp(-\nu_7 x_{34}),
\end{aligned} \tag{48}$$

the state-space model can be derived. The set of coupled nonlinear ODEs

$$\begin{aligned}
\dot{x}_1 &= (2\rho - 1) u_1 x_1,\\
\dot{x}_2 &= u_3 - \lambda_c x_2 + u_2 x_2 - u_4 x_2 + \Phi x_{12},\\
\dot{x}_i &= \lambda_c x_{i-1} - \lambda_c x_i + u_2 x_i - u_4 x_i + \Phi x_{i+10}, \quad \text{for} \quad i = 3,\ldots,11,\\
\dot{x}_i &= u_4 x_{i-10} - \Phi x_i \quad \text{for} \quad i = 12,\ldots,21,\\
\dot{x}_{22} &= u_5 + u_6 x_{22} - \lambda_p x_{22},\\
\dot{x}_i &= \lambda_p x_{i-1} + u_6 x_i - \lambda_p x_i \quad \text{for} \quad i = 23,\ldots,31,\\
\dot{x}_{32} &= u_7 - \lambda_M x_{32},\\
\dot{x}_{33} &= \lambda_M x_{32} - u_8 x_{33},\\
\dot{x}_{34} &= u_9 - \lambda_F x_{34},\\
\dot{x}_{35} &= u_{10} - \lambda_{RegI} x_{35},\\
\dot{x}_{36} &= u_{11} - \lambda_{RegII} x_{36}
\end{aligned} \tag{49}$$

describes the time evolution of the cell count in each compartment. The list of system parameters and a detailed description of the model according to Fliedner and Steinbach can be found in (Hofer *et al.* 1991a; 1991b).

7.2. Constraints. For the system of granulopoiesis, the energy conservation law as in Section 6 cannot be used as a constraint. Instead, a decoupling of compartments is considered. The two compartments CBL and CBM are coupled directly, see Fig. 9. The state equations (49) which represent these compartments can be rewritten as

$$\begin{aligned}
\dot{x}_2 &= u_3 - \lambda_c x_2 + u_2 x_2 - u_4 x_2 + \Phi x_{12},\\
\dot{x}_{l+2} &= \lambda_c x_{l+1} - \lambda_c x_{l+2} + u_2 x_{l+2} - u_4 x_{l+2} + \Phi x_{l+12},\\
\dot{x}_{12} &= u_4 x_2 - \Phi x_{12},\\
\dot{x}_{l+12} &= u_4 x_{l+2} - \Phi x_{l+12}
\end{aligned} \tag{50}$$

for $l = 1,\ldots,9$. The decoupling of the CBL and CBM compartments results in physically motivated constraints. The implementation of the constraints for the blood cell system in VALENCIA-IVP is mathematically the same as for the double pendulum. The constraints are therefore

also denoted by H_H and H_V in the following. The constraint

$$H_{H,l} := x_{l+1} + x_{l+11} \tag{51}$$

for $l = 1, \ldots, 10$ can be expressed in terms of the state variables. The VALENCIA-IVP constraints

$$\dot{H}_{V,l} := \begin{cases} u_3 - \lambda_c x_2 + u_2 x_2 & \text{for } l = 1, \\ \lambda_c x_{l+1} - \lambda_c x_{l+2} + u_2 x_{l+2} & \text{for } l = 2, \ldots, 10 \end{cases} \tag{52}$$

are calculated by integrating the corresponding time derivatives. The simulations will investigate the use of up to $m = 10$ constraints and the influence of the number of constraints on the detection and reduction of overestimation.

7.3. Simulation results. For the dynamic system of granulopoiesis, different settings and their effects on the state enclosures are investigated. For the initial enclosures of the components of the state vector x, the values of Table 3 are used. For all of the simulations, the optimal time t^* is calculated to $t^* = 6.0$ h and the total volume is $V_{total}(t^*) = 7.7864 \cdot 10^{220}$. The step size is set to 0.1. The comparisons are made at $t = t^*$, after the branch and prune algorithm has been applied and the intervals have been merged.

Table 3. Initial values for the state variables of the granulopoiesis model according to Fliedner and Steinbach.

State Variable	i	Initial Value
x_i	$i = 1$	$1.2 \cdot 10^9$
	$i = 2, \ldots, 11$	$8.27 \cdot 10^8$
	$i = 12, \ldots, 22$	$7.52 \cdot 10^5$
	$i = 23, \ldots, 31$	$1.24 \cdot 10^{10}$
	$i = 31, 32$	$2.24 \cdot 10^{11}$
	$i = 34$	$4.0 \cdot 10^{10}$
	$i = 35, 36$	10.0

7.3.1. Optimal subdivision strategy and optimal number of subdivisions. For the dynamic system of granulopoiesis, Strategies 5 and 6 are not applicable because of the high dimensionality $n = 36$ of the system. For that reason, only Strategies 1 through 4 are evaluated for the blood cell system at $t = t^*$. With Strategies 1 and 3, no overestimation could be detected, whereas Strategies 2 and 4 detected an equally large reduction area. In order to be able to compare the efficiency of VALENCIA-IVP for different systems, Strategy 4 is used for the blood cell model, since it was also the most efficient one for the double pendulum.

The effect of the number of subdivisions on the relative reduction area and the computing time are analyzed and the results are recorded in Table 4. An increase in the number of subdivisions causes an increase not only in the relative and absolute reduction areas, but also in the computing time. The simulations have been performed on a standard PC, Intel Pentium 4, 2 GB RAM, hyperthreading enabled, using SuSE Linux 10.3 as the operating system with the compiler gcc 4.3.1. For the granulopoiesis model, 1000 subdivisions are used as the setting for further simulations. The maximum number of subdivisions, 100000, did have the smallest percentage $P_{\texttt{true,undecided}}$, but also the largest computing time.

Table 4. Comparison of the process times and the percentage $P_{\texttt{true, undecided}}$ for different numbers of subdivisions for Strategy 4.

Subdivisions	Computing time	$P_{\texttt{true, undecided}}$
100	28 s	50.84%
1000	30 s	43.64%
10000	302 s	44.47%
100000	67452 s (*)	42.55%

(*) This time is mostly caused by the merging routine.

7.3.2. Effect of the number of constraints. The blood cell model can be simulated with up to $m = 10$ constraints. The previous examinations were for the constraint $m = 1$, see the equations (51) and (52). In Table 5, the results for simulations of the blood cell model with different numbers of constraints can be seen for subdivision Strategy 4 with 1000 subdivisions. The percentage $P_{\texttt{true, undecided}}$ of the area that is true or undecided increases with an increase in the number of constraints. One would expect the opposite, i.e., that an increase in constraints would supply more information and therefore a decrease in the percentage $P_{\texttt{true, undecided}}$. The reason why that is not true is as follows. The subdivision strategies are implemented so that they are not biased towards any component of the state vector. An increase in constraints results in a decrease in the number of subdivisions for each specific component of the state vector. The decrease in subdivisions means that the intervals are larger and therefore the chance that they are outside the VALENCIA-IVP constraints $H_{V,l}$ is smaller. The state $x_{12}(t)$ is included in the constraints. Its enclosure can be

Table 5. Comparison of the number of constraints according to the percentage $P_{\texttt{true, undecided}}$.

Constraints	$V_{\texttt{true,undecided}}$	$P_{\texttt{true, undecided}}$
1	$3.3976 \cdot 10^{220}$	43.64%
2	$3.5449 \cdot 10^{220}$	45.59%
3	$4.3343 \cdot 10^{220}$	55.67%
4	$4.5489 \cdot 10^{220}$	58.42%
5	$6.3210 \cdot 10^{220}$	81.18%

seen in Fig. 10. The branch and prune algorithm is applied at $t = t^*$, resulting in a tighter state enclosure for $t > t^*$.

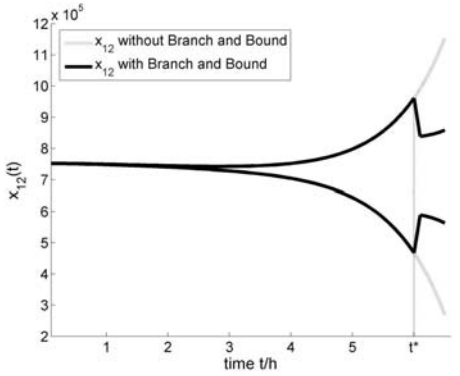

Fig. 10. Enclosure of x_{12} for one constraint.

7.3.3. Seven constraints and a varying number of subdivisions. The previous simulations showed that an increase in the number of constraints for a fixed number of subdivisions resulted in an increase in the percentage $P_{\texttt{true, undecided}}$ due to a reduced number of subdivisions per component of the state vector. The following is an investigation of the effect of an increase in the number of subdivisions on the simulations with the use of multiple constraints. Subdivision Strategy 4 with seven constraints is used as a setting for these simulations. Table 6 records the simulations results. An increase in the number of subdivisions results in a decrease in the percentage $P_{\texttt{true, undecided}}$. For 1000 subdivisions, the branch and prune algorithm was barely able to detect any overestimation. However, it was able to reduce about half of the state enclosure for 100000 subdivisions. This underlines that a larger number of subdivisions results in smaller intervals, which have a higher chance of being detected as `false`. The corresponding total volumes V_{total} of the state enclosure are illustrated in Fig. 11. The total volume of the simulation with 100000 subdivisions is approximately 36% of the total volume with only 1000 subdivisions.

Table 6. Effect of an increase in the number of subdivisions on a simulation using seven constraints.

Number of subdivisions	$P_{\texttt{true, undecided}}$
1000	99.91%
10000	90.16%
100000	55.42%

An increase in the number of constraints should be realized with an increasing number of subdivisions in order for the branch and prune algorithm to work efficiently. The quality of constraints, meaning that they are most sensitive with respect to the variables that cause overestimation, is more important than an abundant number of constraints.

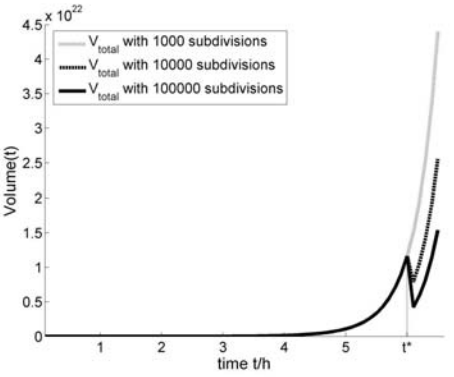

Fig. 11. Total volume V_{total} over the time for simulations with 1000, 10000 and 100000 subdivisions.

7.4. Summary. The investigation of the blood cell model showed that VALENCIA-IVP is applicable to nonlinear, high-dimensional problems. A general approach to find settings that are suitable for the system under consideration can be formulated. First, a mathematical expression for the constraints based on physically motivated techniques needs to be determined. Then, a suitable choice for the subdivision strategy and the number of subdivisions has to be determined, via several simulations with varying settings.

8. Conclusion

In the preceding sections, newly implemented physically motivated techniques for the detection and reduction of overestimation in interval simulations of dynamic systems with uncertainties were introduced, analyzed, and discussed. VALENCIA-IVP is extended with a branch and prune algorithm which is based on physical constraints that can be evaluated in a computationally efficient way.

A method was illustrated with which constraints can be derived for any mechanical system if it is represented in generalized coordinates and if the positive definite and symmetric mass matrix, the time derivative of the generalized coordinates, and the generalized force vector are given. Using this information, the Hamiltonian equations of motion can be obtained for any mechanical system. The Hamiltonian itself is equivalent to the total energy of the mechanical system. Since a mechanical system is subject to the conservation law of energy, the constraints can be used to distinguish between areas which are physically meaningless and meaningful. The branch and prune algorithm uses these constraints to detect and reduce regions that are caused by overestimation. It subdivides *a priori* state enclosures into smaller regions until the region either

conforms to the constraints or not.

The two dynamic systems discussed are a double pendulum and a model of granulopoiesis according to Fliedner and Steinbach. The double pendulum is a classical example of a mechanical system. For the granulopoiesis model, the decoupling of compartments of the cell forming stages were the constraints of the system. The granulopoiesis model is a nonlinear high-dimensional problem. With these two different examples, it was illustrated and underlined that VALENCIA-IVP and its additions are applicable to a variety of real-life problems.

The general framework provided allows the user to generate appropriate constraints based on Hamiltonian system representations. Based on this general foundation, the Hamiltonian can be used as a candidate for Lyapunov functions, which are applicable in tools for controller design. In (van der Schaft, 2005; van der Schaft and Maschke, 2003; Maschke and van der Schaft, 2000), the authors demonstrate such a procedure for a more general formulation of Hamiltonian equations leading to Port-Hamiltonian systems.

In future work, interval arithmetic routines will be implemented to perform stability-based design and analysis of controllers in a verified way.

Acknowledgment

Mareile Freihold would like to thank Andreas Rauh, Chair of Mechatronics, University of Rostock, for supporting her throughout this work. Furthermore, the authors would like to thank the reviewers for their helpful suggestions for improving of this paper.

This work was performed while Mareile Freihold was with the Institute of Measurement, Control, and Microtechnology, University of Ulm, Germany.

References

Bendsten, C. and Staunting, O. (2007). FADBAD++, Version 2.1, Available at: `http://www.fadbad.com/fadbad.html`.

Boyd, S., Gosh, A. and Magnani, A. (2003). Branch and bound methods, Available at: `http://www.stanford.edu/class/ee392o/bb.pdf`.

Clausen, J. (1999). Branch and bound algorithms: Principles and examples, Available at: `citeseer.ist.psu.edu/683497.html`.

de Figueiredo, L. H., van Iwaarden, R. and Stolfi, J. (1997). Fast interval branch-and-bound methods for unconstrained global optimization with affine arithmetic, *Technical Report IC-97-08*, Institute of Computing, University of Campinas, Campinas, Brazil.

Hofer, E. P., Fan, Y. and Tibken, B. (1991a). Extraction of rules for model based estimation of granulocytopoiesis, *in* M. Frik (Ed.), *5th German-Japanese Seminar Nonlinear Problems in Dynamical Systems—Theory and Applications*, Daun, Vulkaneifel, pp. 58–68.

Hofer, E. P., Tibken, B. and Fliedner, T. M. (1991b). Modern control theory as a tool to describe the biomathematical model of granulocytopoiesis, *in* D. Möller and O. Richter (Eds.), *Analyse dynamischer Systeme in Medizin, Biologie, Ökologie*, Vol. 275, Springer-Verlag, Berlin, pp. 33–39.

Kearfott, R. B. (1992). An interval branch and bound algorithm for bound constrained optimization problems, *Journal of Global Optimization* **2**(3): 259–280.

Keil, C. (2007). PROFIL/BIAS, Version 2.0.4, Available at: `http://www.ti3.tu-harburg.de/keil/profil/`.

Maschke, B. M. and van der Schaft, A. J. (2000). Portcontrolled Hamiltonian representation of distributed parameter systems, *in* N. E. Leonard and R. Ortega (Eds.), *Proceedings of the IFAC Workshop on Lagrangian and Hamiltonian Methods for Nonlinear Control, Princeton, NJ, USA*, pp. 28–38.

Moore, R. E. (1964). *Error in Digital Computation, the Automatic Analysis and Control of Error*, John Wiley & Sons, New York, NY.

Nedialkov, N. S. (2007). Interval tools for ODEs and DAEs, *CD-Proceedings of the 12th GAMM-IMACS International Symposium on Scientific Computing, Computer Arithmetic, and Validated Numerics SCAN 2006, Duisburg, Germany*, IEEE Computer Society, Los Alamitos, CA.

Pfeiffer, F. and Reithmeier, E. (1987). *Roboterdynamik*, Teubner, Stuttgart, (in German).

Rauh, A. (2008). *Theorie und Anwendung von Intervallmethoden für Analyse und Entwurf robuster und optimaler Regelungen dynamischer Systeme*, Fortschritt-Berichte VDI, Reihe 8, Nr. 1148, PhD thesis, University of Ulm, Ulm, (in German).

Rauh, A., Auer, E. and Hofer, E. P. (2007). ValEncIA-IVP: A comparison with other initial value problem solvers, *CD-Proceedings of the 12th GAMM-IMACS International Symposium on Scientific Computing, Computer Arithmetic, and Validated Numerics SCAN 2006, Duisburg, Germany*, IEEE Computer Society, Los Alamitos, CA.

Rauh, A., Brill, M. and Günther, C. (2009). A novel interval arithmetic approach for solving differential-algebraic equations with VALENCIA-IVP, *International Journal of Applied Mathematics and Computer Science* **19**(3): 381–397.

Singer, A. B. and Barton, P. I. (2006). Bounding the solutions of parameter dependent nonlinear ordinary differential equations, *SIAM Journal on Scientific Computing* **27**(6): 2167–2182.

The American Heritage Medical Dictionary (2007). Houghton Mifflin Company, Boston, MA.

van der Schaft, A. J. (2005). Network modeling and control of physical systems, DISC theory of port-Hamiltonian systems, Available at: `http://www.vf.utwente.nl/~schaftaj/downloads-diversen/DISCportbased1.pdf`.

van der Schaft, A. J. and Maschke, B. M. J. (2003). Port-Hamiltonian systems: A theory for modeling, simulation and control of complex physical systems, Available at: `http://www-lar.deis.unibo.it/euron-geoplex-sumsch/files/lectures_1/Van Der Schaft/VDSchaft_01_PCHS.pdf`.

Mareile Freihold received her diploma degree in electrical engineering in 2008 from the University of Ulm, Germany (*The detection and reduction of overestimation of interval simulations with uncertainties with physically motivated constraints*). Currently, she works for Daimler AG in the truck section for the development of cockpit instrumentations.

Eberhard P. Hofer is a retired director of the Institute of Measurement, Control, and Microtechnology at the University of Ulm, Germany. He received his doctorate in optimal control and his habilitation qualification in engineering cybernetics from the University of Stuttgart. He has worked for industry (in Germany and the USA) as a project manager in process control and software engineering. He has been a visiting professor at IBM, UC Berkeley, Waseda University in Tokyo, Kobe University, and the Japan Advanced Institute of Science and Technology. interval methods with applications to technical and biomedical systems. For his achievements he has received numerous research awards in applied sciences.

Received: 22 September 2008
Revised: 15 December 2008